Journal of Superconductivity and Novel Magnetism
https://doi.org/10.1007/s10948-024-06800-y

RESEARCH

Anisotropic Inverse Spin Hall Effect Observed in Sputtering Grown Topological Antiferromagnet Mn_3Sn Films

Dengfu Deng[1,3] · Dong Gao[1,3] · Shuyao Chen[1,3] · Yunfei Xie[1,3] · Jiayi zheng[1,3] · Lintong Huang[1,3] · Chenjie Zhang[1,3] · Donghua Liu[2] · Lei Bi[1,3] · Tao Liu[1,3]

Received: 5 April 2024 / Accepted: 4 July 2024

Abstract

Recent theoretically predicted strong anisotropic spin Hall effect (SHE) or inverse SHE (ISHE) in chiral antiferromagnetic compounds Mn_3X (X = Ge, Sn, Ga, Ir, Rh, and Pt) could potentially expand the horizons of the antiferromagnet spintronics; however, it has not been experimentally observed yet. For achieving this goal, we have first successfully fabricated high-quality Kagome phase Mn_3Sn films with smooth surface by a combination of room-temperature magnetron sputtering and high-temperate annealing. These Mn_3Sn films were proved to be epitaxially grown on MgO (110) single crystal substrate with a seldom reported $(10\bar{1}0)$ orientation that could serve as a good platform for the studies of the crystalline orientation-related anisotropic phenomenon. Then, by employing spin pumping-induced inverse spin Hall effect (SP-ISHE) voltage measurements, we have experimentally proved the existence of crystalline orientation-related anisotropic ISHE with an amplitude of more than 35% in our Mn_3Sn films.

Keywords Anisotropic inverse spin Hall effect · Mn_3Sn thin films · Magnetron sputtering

1 Introduction

Spin Hall effect (SHE) [1–3] can convert charge current flowing in a metal layer to transverse spin current, providing an energy-efficient method to electrically control the magnetization in the adjacent magnetic layers. This makes SHE become a key element of modern spintronics [4]. Conventional SHE was widely reported in heavy metal films and was isotropic [5–7]. However, it is recently theoretically predicted that there is an existence of large anisotropic SHE in a type of chiral antiferromagnetic compound Mn_3X (X = Ge, Sn, Ga, Ir, Rh, and Pt) that could both be related to their crystal structure and inverse triangular magnetic structure [8, 9]. Mn_3X is also antiferromagnetic Weyl semimetal [10, 11] that possesses an unusual combination of magnetic, magneto-electric, magneto-optical, and topological properties [12–16]. For instance, a surprisingly large anomalous Hall effect (AHE) [17–19] and magneto-optic Kerr effect (MOKE) [20], comparable in size to that of transition metal ferromagnets, were experimentally detected in these materials even though they have almost no net moment. This new anisotropic SHE in chiral antiferromagnet could potentially expand the horizons of antiferromagnetic spintronics and therefore has attracted great research interest. There have already been experiments reporting the observation of magnetic order-related anisotropy of SHE in Mn_3Sn that was termed magnetic SHE (MSHE) [21–23]. However, no counterpart experiment work regarding the anisotropy of SHE related to crystalline orientations, that is important as well from the view side of both fundamental studies and device applications, has been carried out.

Under this context, we have first successfully fabricated high-quality Kagome phase Mn_3Sn films with a smooth surface by a combination of room-temperature magnetron sputtering and high-temperate annealing. These Mn_3Sn films were proved to be epitaxially grown on MgO (110) single crystal substrate with a seldom reported $(10\bar{1}0)$ orientation

✉ Tao Liu
liu.tao@uestc.edu.cn

1 School of Electronic Science and Engineering, University of Electronic Science and Technology of China, Chengdu 611731, China

2 School of Materials and Energy, University of Electronic Science and Technology of China, Chengdu 610054, China

3 National Engineering Research Center of Electromagnetic Radiation Control Materials, University of Electronic Science and Technology of China, Chengdu 611731, China

Published online: 13 July 2024

that could serve as a good platform for the studies of the crystalline orientation-related anisotropic phenomenon. Then, after further depositing of a NiFe layer, we achieved evidence of the existence of crystalline-related anisotropic SHE with an amplitude of more than 35% in these Mn_3Sn films by measuring the corresponding inverse effect, i.e., the inverse spin Hall effect (ISHE).

2 Methods

Mn_3Sn films of 40 nm thickness were deposited on MgO (110) single crystal substrates by DC magnetron sputtering at a rate of 0.27 Å/s. The base pressure of the sputtering chamber was better than 2×10^{-5} Pa, and the working gas was high pure Ar at a pressure of 0.3 Pa. To achieve well-crystallized Mn_3Sn films with smooth surfaces, these Mn_3Sn films were deposited at room temperature and then annealed under different temperature ranges from 600 to 720 °C. For the Mn_3Sn films annealed at 600 and 640 °C, an additional 10 nm-thick NiFe layer was deposited after the sample cooled down to room temperature. All samples were covered with a 2 nm-thick SiO_2-protecting capping layer. The NiFe layers were grown at a rate of 0.65 Å/s by DC sputtering with 0.6 Pa Ar working gas, and the SiO_2 layers were grown at a rate of 0.21 Å/s using an RF power source with 0.3 Pa Ar working gas. For Mn_3Sn/SiO_2 samples, the components, crystal structure, surface morphology, and anomalous Hall resistance were measured by energy-dispersive X-ray spectroscopy (EDS), high-resolution X-ray diffraction (XRD), atomic force microscopy (AFM), and physical property measurement system (PPMS), respectively. For $Mn_3Sn/NiFe/SiO_2$ samples, the inverse spin Hall effect (ISHE) was tested by a spin pumping measurement method we reported before [24].

3 Results and Discussion

Figure 1a shows the EDS pattern, from which the atomic ratio of Mn:Sn in our Mn_3Sn film is determined to be 3.13:1, with Mn slightly over-stoichiometric, that could help stabilize the Kagome phase, as previously reported [25]. Figure 1b presents the XRD spectrums of the Mn_3Sn films annealed under different temperatures. From the diagram, the diffraction peak of Kagome phase Mn_3Sn $(30\bar{3}0)$ appeared evidently at 640 ~ 720 °C, but inconspicuously at 600 °C, which implies that our film crystallization temperature is above 600 °C. Moreover, as the temperature is raised from 640 to 720 °C, the strength of the Mn_3Sn $(30\bar{3}0)$ diffraction peak gradually increases. This indicates

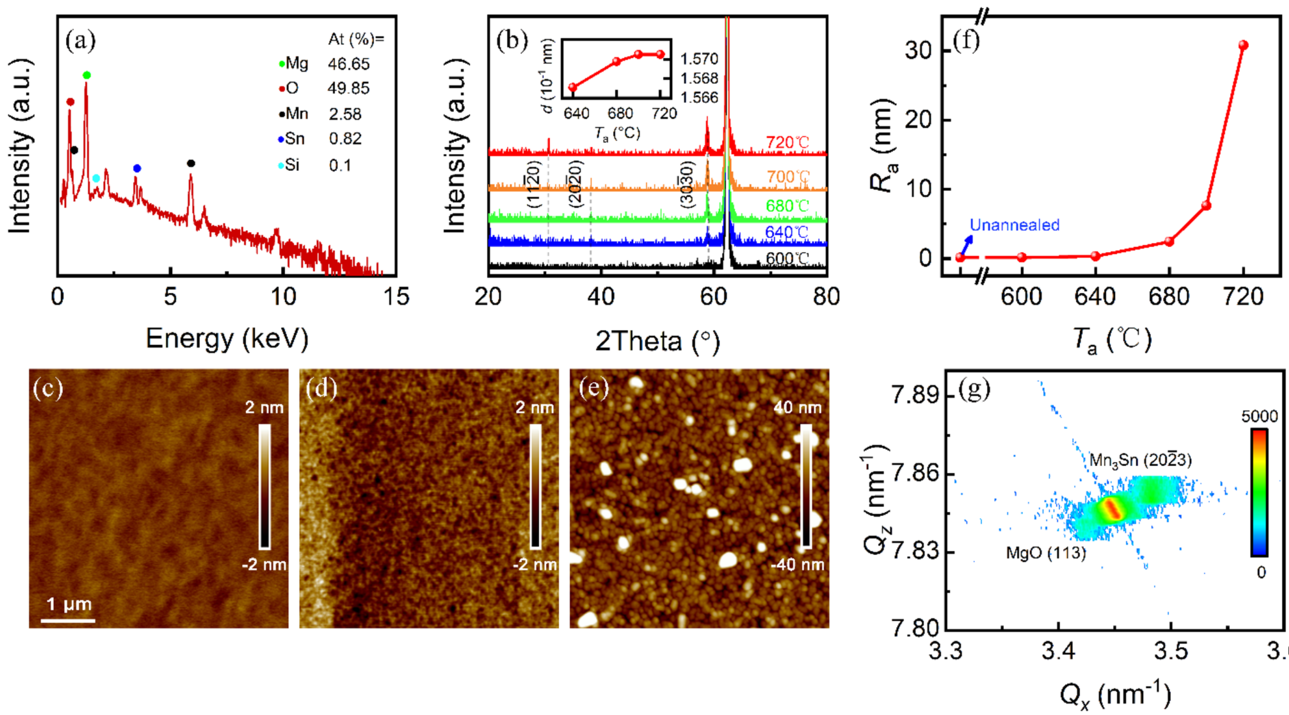

Fig. 1 **a** EDS spectra of a room temperature sputtered Mn_3Sn thin film. **b** 2θ-ω XRD spectra and **c**–**e** AFM images of Mn_3Sn thin film annealed at different temperatures (T_a). **f** Roughness (R_a) v.s. T_a. **g** RSM spectra of a 640 °C annealed Mn_3Sn thin film. The inset in **b** is the calculated out-of-plane lattice constant change with T_a

a progressive growth of the grain size. However, the (30$\bar{3}$0) peak position also slightly shifts to the left with increasing temperature, which means the out-of-plane lattice constant (d) of Mn_3Sn film increases as elevating the annealing temperature (T_a), as illustrated in the inset of Fig. 1b. Most probably, there is a gradual stress release, that became more severe at higher temperature, happened during the annealing process. Moreover, another weak diffraction peak of (11 $\bar{2}$ 0) with different crystal orientation became visible at 720 °C. These results imply that excessive annealing temperature could be harmful to the homogeneity and even epitaxial nature of our Mn_3Sn films.

In order to determine the optimal annealing temperature, we have further studied the surface morphology of these annealed Mn_3Sn samples that represent one of the most important properties of the thin films for device applications. Figure 1c–e shows the AFM diagram of samples annealed at 600 °C, 640 °C, and 700 °C, respectively, and Fig. 1f summarizes how their average roughness (R_a) changes with annealing temperature. As shown, the grain size gradually increases with the increase of annealing temperature, confirming the enhancement of the degree of crystallization. However, R_a is found to increase very quickly as the annealing temperature elevates, especially after 680 °C. All of these results are consistent with the conclusion of the above XRD results. As a result, highly homogeneous (30$\bar{3}$0) oriented Mn_3Sn films with desirable smooth surface can only be obtained under the annealing temperature of around 640 °C, which is exactly the sample we will focus on in the following studies.

For further clarifying if these Mn_3Sn samples annealed under 640 °C possessing enough good quality to support the final goal of this work, i.e., study of the crystal structure related anisotropy SHE, we also carried out the high-resolution reciprocal space map (RSM) and anomalous Hall resistance measurements. Figure 1g presents the RSM results around the MgO (113) peak. Except for this diffraction peak from the MgO substrate, another peak corresponding to Mn_3Sn (20$\bar{2}$3) near the right and upper of the peak MgO (113) can also be well distinguished. Unambiguously, this indicates the epitaxial growth nature of this Mn_3Sn film along the MgO substrate surface.

Figure 2 shows the field dependence of anomalous Hall resistivity ρ_H measured at room temperature by the van der Pauw method, with the current of $I = 1$ mA applied along the diagonal direction of a 5 mm × 5 mm square sample. The details of the measurement are presented in the configuration of the inset in Fig. 2. Upon reversing the magnetic field, a clear hysteresis behavior in the Hall resistivity is observed. The saturation anomalous Hall resistivity is ~ 1.2 μ Ω • cm and coercivity is ~ 3500 Oe, which are close to the reported values of the epitaxial grown Mn_3Sn thin films [26–30]. This is good evidence indicating that there is sufficient topological nature in this Mn_3Sn thin film.

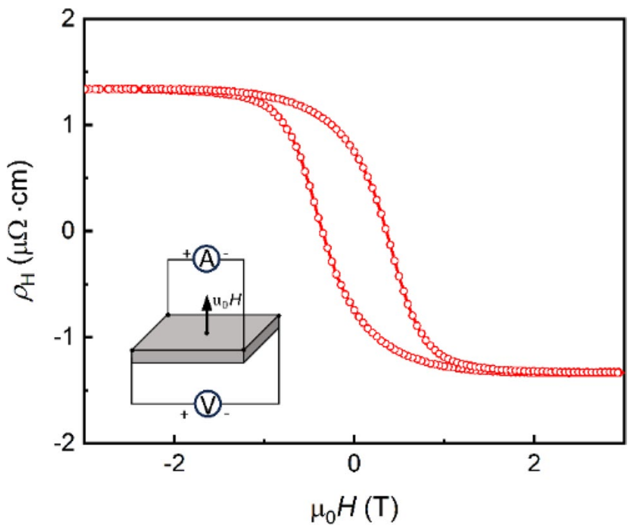

Fig. 2 The ρ_H v.s. H loop of a Mn_3Sn film annealed at 640 °C measured at room temperature. The inset is a diagram for the measurement setup

Based on the achievement of this high-quality epitaxial grown Mn_3Sn thin film with unique (10$\bar{1}$0) orientation, we could, in the next, experimentally test the predicted crystal orientation related anisotropic SHE in Ref. 8. In order to quantitatively compare the SHE of this Mn_3Sn thin film along different crystalline directions, we measured the spin pumping-induced ISHE voltage (V_{ISHE}) using a setup we developed and reported before [24], the configuration of which is shown in Fig. 3a. To carry out this measurement, a 10 nm-thick NiFe layer was deposited on the Mn_3Sn film for the objective of pumping spin current to the Mn_3Sn layer along the film thickness direction, as the moments of NiFe layer are driven to be ferromagnetic resonance (FMR) by RF microwave field h_{rf} (red double arrow). Additionally, for better comparison with the predicted anisotropic SHE values in Ref. 8, we defined the coordination according to the crystalline orientation and set x, y, and z axis in the same manner as Ref. 8, i.e., x ‖ [10$\bar{1}$0], the y ‖ [1$\bar{2}$10], and z ‖ [0001]. Then, using a 5 mm × 5 mm square sample, with edges parallel to y (or [1$\bar{2}$10] direction) and z (or [0001] direction), by rotating the sample according to the nominal axis, i.e., adjusting the angle of φ that representing the relative angle between the applied magnetic field (or the moment of NiFe layer) and the z axis, one can obtain the V_{ISHE} produced from the different crystalline direction. Since ISHE (or SHE) is quantified by the spin Hall angle (θ_{SH}), and both our measured V_{ISHE} and the Ref. 8 calculated spin Hall conductivity (σ) are proportional to θ_{SH} [31, 32], we could define the anisotropy of ISHE (or SHE) between the cases

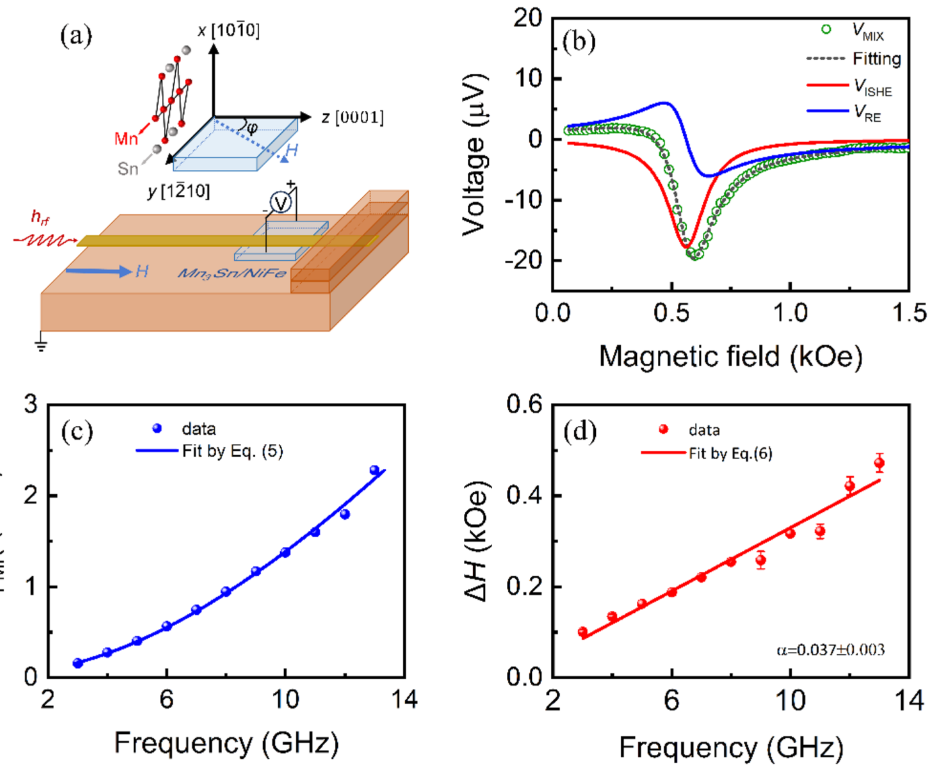

Fig. 3 **a** Diagram of the spin pumping-induced ISHE (SP-ISHE) voltage measurement setup. **b** SP-ISHE voltage measurement and data analysis results obtained at $\varphi = 0°$; the green dots are experiment-measured V_{MIX}, the black-dashed line is a fit to Eq. (2), the red and blue lines are the exacted V_{ISHE} and V_{RE}; **c** and **d** are the summarized of the fits of V_{MIX} yielded ΔH_{FMR} and ΔH at different applied microwave frequency. The error bars represent the standard deviation values of the fittings

of the magnetic field applied along φ_1 and φ_2 directions ($\Delta_{ISHE}(\varphi_1, \varphi_2)$) as

$$\Delta_{ISHE}(\varphi_1,\varphi_2) = \frac{|\theta_{SH}(\varphi_1)| - |\theta_{SH}(\varphi_2)|}{|\theta_{SH}(\varphi_2)|} = \frac{|\sigma(\varphi_1)| - |\sigma(\varphi_2)|}{|\sigma(\varphi_2)|} = \frac{|V_{ISHE}(\varphi_1)| - |V_{ISHE}(\varphi_2)|}{|V_{ISHE}(\varphi_2)|} \tag{1}$$

where $\sigma(\varphi)$ represents the spin Hall conductivity at φ; and $V_{ISHE}(\varphi)$ represents measured V_{ISHE} at φ. It needs to be noted that in order to minimize the uncertainty caused by the sample dimension, we will, in the following, only focus on the case of $\varphi = 0°$, 90°, 180°, and 270° that correspond to the predicted σ^z_{xy}, σ^y_{xz}, $\sigma^z_{x(-y)}$, and $\sigma^y_{x(-z)}$, in Ref. 8, respectively.

Figure 3b shows the representative measurement and analytic result obtained at $\varphi = 0°$, with the applied driving microwave at a frequency of 6 GHz and power of 25 dBm. The green dots are the measured DC voltage signal (V_{MIX}). As illustrated in the previous works [33–35], V_{MIX} contains the contributions from both ISHE (V_{ISHE}) in the Mn_3Sn layer and magnetoresistance (or Ouster field) caused rectification effect (V_{RE}) in the metallic NiFe magnetic layer. To separate V_{ISHE} from V_{MIX}, one can fit the curve of V_{MIX} versus magnetic field (H) by the following Eq. (2) [34, 35]:

$$V_{MIX} = S\frac{\Delta H^2}{\Delta H^2 + (H - H_{FMR})^2} + A\frac{2\Delta H(H - H_{FMR})}{\Delta H^2 + (H - H_{FMR})^2} + V_B \tag{2}$$

where the first, second, and third term on the right are a symmetric Lorentz function, an asymmetric Lorentz function, and a constant that are the respective contributions of V_{ISHE}, V_{RE}, and background signal, i.e.

$$V_{ISHE} = S\frac{\Delta H^2}{\Delta H^2 + (H - H_{FMR})^2} \tag{3}$$

$$V_{RE} = A\frac{2\Delta H(H - H_{FMR})}{\Delta H^2 + (H - H_{FMR})^2} \tag{4}$$

S and A stand for the symmetric and asymmetric Lorentz coefficient, respectively; ΔH and H_{FMR} are the FMR linewidth and FMR field, respectively. The black-dashed line shown in Fig. 3b is a fit of V_{MIX} versus H curve to Eq. (2). From the fitting, the symmetric V_{ISHE} term (red line) and asymmetric term V_{RE} (blue line) were separated; besides, ΔH and H_{FMR}, the magnetic parameters of NiFe layer, were also determined from the fitting to be $0.19 \pm 7 \times 10^{-4}$ kOe and $0.56 \pm 3 \times 10^{-4}$ kOe, respectively.

To further indicate the feasibility of the above approach we used for analyzing V_{MIX} and checking the quality of our fabricated NiFe films, the fits which yielded H_{FMR} and ΔH

at different applied microwave frequency (f) were summarized in Fig. 3c, d and fitted by Kittel formulas [36]:

$$f = |\gamma|[H_{FMR}(H_{FMR} + 4\pi M_S)]^{\frac{1}{2}} \quad (5)$$

$$\Delta H = \frac{\alpha f}{|\gamma|} + H_0 \quad (6)$$

where $|\gamma|$, $4\pi M_S$, ΔH_0, and α are the gyromagnetic ratio, effective saturation magnetization, inhomogeneity line broadening, and Gilbert damping, respectively. As shown, both results can be fitted well, and the fittings yield $|\gamma| = 1.51 \pm 0.16$ MHz/Oe, $4\pi M_S = 10{,}494 \pm 600$ G, $\Delta H_0 = 4.08 \pm 2.23$ Oe, and $\alpha = 0.037 \pm 0.003$. All of these parameters are very close to that of previously reported permalloy thin films [31, 37]. In particular, this α represents a very reasonable value for a high-quality polycrystal magnetic metal thin film.

Figure 4a presents the obtained V_{ISHE} versus H curves for the Mn_3Sn/NiFe sample with the Mn_3Sn layer annealed at 640 °C. It is apparent that the amplitude of V_{ISHE}, along different crystal directions, is different, especially for the case between $\varphi = 0°$ (or 180°) and $\varphi = 90°$ (or 270°), indicating the existence of considerable crystal orientation related anisotropic ISHE (or SHE) in the Mn_3Sn layer of this sample. At $\varphi = 0°$, 90°, 180°, and 270°, the amplitude of $V_{ISHE} = -21.4$ μV, -15.7 μV, 18.5 μV, and 14.2 μV respectively. Then, the experimentally measured anisotropy of ISHE in our 640 °C annealed Mn_3Sn film could be calculated by Eq. (1), that is

$$\Delta_{ISHE}(0°, 90°) = \frac{|V_{ISHE}(0°)| - |V_{ISHE}(90°)|}{|V_{ISHE}(90°)|} = 36.3\% \quad ;$$

$$\Delta_{ISHE}(180°, 270°) = \frac{|V_{ISHE}(180°)| - |V_{ISHE}(270°)|}{|V_{ISHE}(270°)|} = 30.3\%$$

As illustrated above, the correspondence theoretically predicted anisotropy of ISHE in single crystal Mn_3Sn by Ref. 8 can be calculated as well by Eq. (1), that is

$$\Delta_{ISHE}(0°, 90°) = \Delta_{ISHE}(180°, 270°) = \frac{|\sigma(0°)| - |\sigma(90°)|}{|(\sigma 90°)|} = \frac{|\sigma^z_{xy}| - |\sigma^y_{xz}|}{|\sigma^y_{xz}|} = \frac{64 - 36}{36} = 77.7\%$$

It could be seen that the experimentally measured anisotropy of ISHE in our 640 °C annealed Mn_3Sn film and that of the predicted value in single crystal Mn_3Sn have the same sign, and their amplitudes are also in the same magnitude

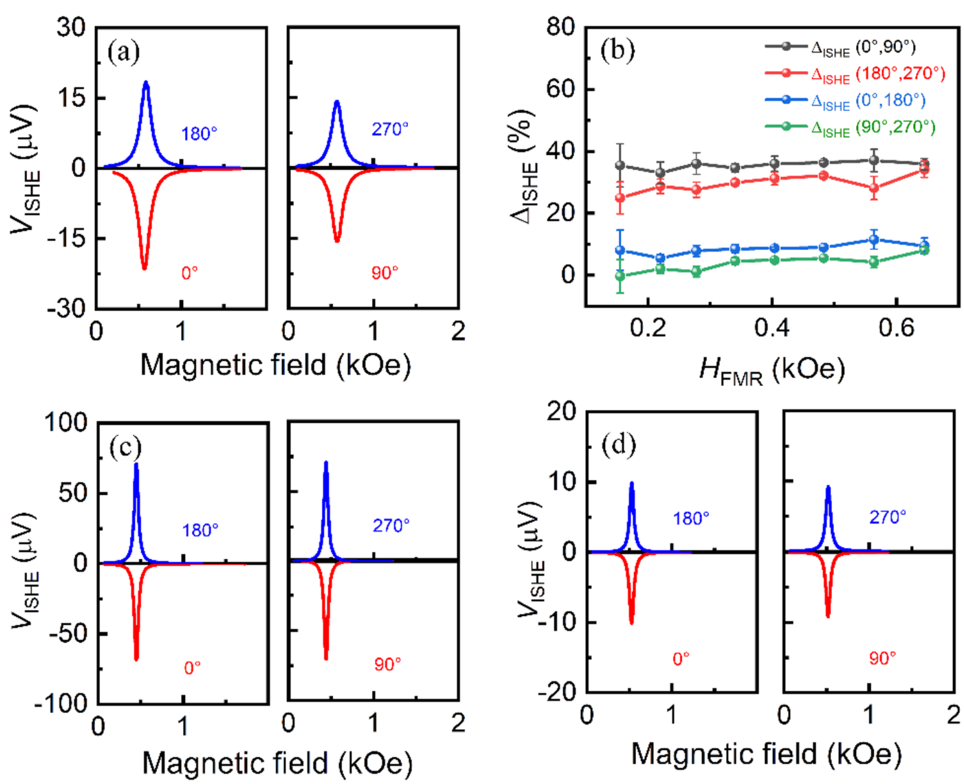

Fig. 4 **a** V_{ISHE} v.s. H curves obtained at four different φ angles; **b** Δ_{ISHE} v.s. H_{FMR} of 640 °C annealed Mn_3Sn/NiFe; **c** V_{ISHE} v.s. H curves of Pt/NiFe; **d** 600 °C annealed Mn_3Sn/NiFe. The error bars in **b** were obtained by repeating the same angle dependence SP-ISHE measurement five times after re-wiring the same sample

of order, consistent considerably well with each other. We would like to emphasize that there were already experiment observation reporting the sign reversing of ISHE (or SHE) in Mn_3X or other chiral antiferromagnets as the reversing of their octuple vector [21]. This effect was termed MSHE [21–23], that is actually the magnetic order- and orientation-related anisotropic SHE (or ISHE). The crystalline structure and orientation-related anisotropic SHE (or ISHE), that is also important for the exploration of new spintronic devices or the optimization of their properties, however, have not been experimentally studied yet. In the case of our Mn_3Sn/NiFe sample, the spin pumping measurements were carried out immediately after the sample fabrication (including a high-temperature annealing process), without saturating the octuple vector in a large out-of-plane magnetic field. In addition, the influence of the applied small in-plane magnetic field during spin pumping measurements on the orientation of the octuple vector is also neglectable, which could be approved in a control experiment that will be discussed shortly below. Therefore, the Mn_3Sn layer was kept in a demagnetization state, and the anisotropic ISHE we observed could be unambiguously ascribed to the crystalline structure and orientation-related anisotropic ISHE.

In order to further confirm the anisotropic spin pumping-induced DC voltage we observed has not resulted from any measurement-related parasitic effect, we further carried out the following three control experiments. Firstly, a Kagome plane scattering resulted similar amount of ~ 33% longitudinal resistivity enhancement along [0001] direction (z-axis in our case) was observed in the Mn_3Sn single crystal of Ref. [18]. Therefore, we have carefully measured the longitudinal resistivity of our Mn_3Sn thin film both in the Mn_3Sn/NiFe bilayer or a 40 nm-thick Mn_3Sn single layer prepared under the same condition. It reveals that the resistivity of Mn_3Sn in a single-Mn_3Sn layer (or Mn_3Sn/NiFe bilayer) is 448 μΩ•cm (420 μΩ•cm) and 457 μΩ•cm (428 μΩ•cm) along y- and z-axis, respectively. Apparently, the anisotropy of the longitudinal resistivity in our Mn_3Sn films is very weak and can almost be neglected. It is not very clear whether the reason for the absence of the Kagome plane scattering resulted from anisotropic resistivity in our Mn_3Sn films, but one possible explanation could be the increase of crystalline unrelated scatterings in epitaxial thin film, like scattering at grain boundary or two interfaces, which have seriously weakened this anisotropic scattering effect. Nevertheless, it is safe to conclude from the above results that the anisotropic V_{ISHE} we measured in Mn_3Sn/NiFe has nothing to do with the anisotropy of longitudinal resistivity in Mn_3Sn. Secondly, we carried out the angle-dependent SP-ISHE measurements at lower frequencies, so that the FMR could occur at a lower magnetic field to minimize the influence of the applied in-plane field on the orientation of the out-of-plane octuple vector. The obtained four different Δ_{ISHE} as a function of H_{FMR} are presented in Fig. 4b. As shown, no obvious change of Δ_{ISHE} as H_{FMR} could be observed. This proves that the anisotropic V_{ISHE} we measured is not related to the applied magnetic field caused by the tilting of the octuple vector. Thirdly, we prepared another two control samples, with the well-crystallized Mn_3Sn layer in the Mn_3Sn (40)/NiFe (10) sample discussed above, replaced by a 4 nm-thick Pt layer or an amorphous Mn_3Sn layer that annealed under a lower temperature of 600 °C. The V_{ISHE} versus H curves of these two control samples, that were extracted from the measured V_{MIX}, are shown in Fig. 4b, c. As presented, only very weak anisotropy, with an amplitude of less than 2%, could be observed in these two control samples. This indicates that the anisotropic V_{ISHE} detected in our 640 °C annealed Mn_3Sn film is strongly related to its epitaxial growth nature and is a result of the crystalline structure and orientation-leaded anisotropic ISHE.

4 Conclusions

In summary, well-crystallized Mn_3Sn thin films with smooth surface were obtained on MgO(110) substrates by a combination of room-temperature magnetron sputtering and high-temperature post-annealing. These Mn_3Sn thin films were proved to be epitaxially grown on MgO single crystal substrates with a seldom reported $(10\bar{1}0)$ orientation. By carrying out spin pumping-induced inverse spin Hall voltage measurement, we observed the anisotropy of the inverse spin Hall effect, with an amplitude of more than 35%, in a 640 °C annealed Mn_3Sn thin film. This is the first time experimentally observation of the crystalline structure and orientation-related anisotropic SHE (or ISHE) in chiral antiferromagnetic materials.

Author Contribution DD, DG, LH, and CZ fabricated and characterized all the samples. DD, SC, and YX performed SP-ISHE voltage measurements. All authors participated in the data analyses. TL formulated the problem and designed the study. TL, DL, and LB managed the project. DD and TL prepared the manuscript, with the help from all the other authors.

Funding This work was supported by the Ministry of Science and Technology of the People's Republic of China (grant no. 2021YFB2801600), the National Natural Science Foundation of China (grant no. 52072060, 52202164, 52021001, U22A20148, and 52102357), and the Natural Science Foundation of Sichuan (grant no. 2023NSFSC1950 and 2022NSFSC1990).

Data Availability No datasets were generated or analyzed during the current study.

Declarations

Conflict of Interest The authors declare no competing interests.

References

1. Hirsch, J.E.: Spin Hall effect. Phys. Rev. Lett. **83**, 1834–1837 (1999)
2. Zhang, S.: Spin Hall effect in the presence of spin diffusion. Phys. Rev. Lett. **85**, 393–396 (2000)
3. Sinova, J., Culcer, D., Niu, Q., Sinitsyn, N.A., Jungwirth, T., MacDonald, A.H.: Universal intrinsic spin Hall effect. Phys. Rev. Lett. **92**(12), 126603 (2004)
4. Jungwirth, T., Wunderlich, J., Olejník, K.: Spin Hall effect devices. Nat. Mater. **11**(5), 382–390 (2012)
5. Wunderlich, J., Kaestner, B., Sinova, J., Jungwirth, T.: Experimental observation of the spin-Hall effect in a two-dimensional spin–orbit coupled semiconductor system. Phys. Rev. Lett. **94**, 047204 (2005)
6. Valenzuela, S.O., Tinkham, M.: Direct electronic measurement of the Spin Hall effect. Nature **442**, 176–179 (2006)
7. Sinova, J., Valenzuela, S.O., Wunderlich, J., Back, C.H., Jungwirth, T.: Spin Hall effects. Rev. Mod. Phys. **87**(4), 1213 (2015)
8. Zhang, Y., Sun, Y., Yang, H., Železný, J., Parkin, S.P., Felser, C., Yan, B.: Strong anisotropic anomalous Hall effect and spin Hall effect in the chiral antiferromagnetic compounds Mn_3X (X= Ge, Sn, Ga, Ir, Rh, and Pt). Phys. Rev. B **95**(7), 075128 (2017)
9. Železný, J., Zhang, Y., Felser, C., Yan, B.: Spin-polarized current in noncollinear antiferromagnets. Phys. Rev. Lett. **119**(18), 187204 (2017)
10. Cable, J.W., Wakabayashi, N., Radhakrishna, P.: Magnetic excitations in the triangular antiferromagnets Mn_3 Sn and Mn_3 Ge. Phys. Rev. B **48**, 6159–6166 (1993)
11. Tomiyoshi, S., Yamaguchi, Y.: Magnetic structure and weak ferromagnetism of Mn_3Sn studied by polarized neutron diffraction. J. Phys. Soc. Japan **51**(8), 2478–2486 (1982)
12. Higo, T., Nakatsuji, S.: Thin film properties of the non-collinear Weyl antiferromagnet Mn3Sn. J. Magn. Magn. Mater. 170176 (2022)
13. Nagaosa, N., Sinova, J., Onoda, S., MacDonald, A.H., Ong, N.P.: Anomalous Hall effect. Rev. Mod. Phys. **82**(2), 1539 (2010)
14. Tsai, H., Higo, T., Kondou, K., Nomoto, T., Sakai, A., Kobayashi, A., Nakano, K., Yakushili, K., Arita, R., Miwa, S., Otani, Y., Nakatsuji, S.: Electrical manipulation of a topological antiferromagnetic state. Nature **580**(7805), 608–613 (2020)
15. Tsai, H., Higo, T., Kondou, K., Kobayashi, A., Nakano, T., Yakushiji, K., Miwa, S., Otani, Y., Nakatsuji, S.: Spin–orbit torque switching of the antiferromagnetic state in polycrystalline Mn3Sn/Cu/heavy metal heterostructures. AIP Adv. **11** (4) (2021)
16. Takeuchi, Y., Yamane, Y., Yoon, J.Y., Itoh, R., Jinnai, B., Kanai, S., Leda, J., Fukami, S., Ohno, H.: Chiral-spin rotation of non-collinear antiferromagnet by spin–orbit torque. Nat. Mater. **20**(10), 1364–1370 (2021)
17. Chen, H., Niu, Q., MacDonald, A.H.: Anomalous Hall effect arising from noncollinear antiferromagnetism. Phys. Rev. Lett. **112**(1), 017205 (2014)
18. Nakatsuji, S., Kiyohara, N., Higo, T.: Large anomalous Hall effect in a non-collinear antiferromagnet at room temperature. Nature **527**, 212–215 (2015)
19. Liu, J.J., Meng, K.K., Chen, J.K., Wu, Y., Miao, J., Xu, X.G., Jiang, Y.: Robust interface-induced unusual anomalous Hall effect in Mn_3Sn/Pt bilayers. Rare Met. **41**(9), 3012–3018 (2022)
20. Higo, T., Man, H., Gopman, D.B., Wu, L., Koretsune, T., van't Erve, O.M., Kabanov, Y.P., Rees, D., Li, Y., Suzuki, M., Patankar, S., Ikhlas, M., Chien, L.C., Arita, R., Shull, R.D., Orenstein, J., Nakatsuji, S.: Large magneto-optical Kerr effect and imaging of magnetic octupole domains in an antiferromagnetic metal. Nat. Photonics. **12**(2), 73–78 (2018)
21. Kimata, M., Chen, H., Kondou, K., Sugimoto, S., Muduli, P.K., Ikhlas, M., Omori, Y., Tomita, T., MacDonald, A.K., Nakatsuji, S., Otani, Y.: Magnetic and magnetic inverse spin Hall effects in a noncollinear antiferromagnet. Nature **565**(7741), 627–630 (2019)
22. Hu, S., Shao, D.F., Yang, H., Pan, C., Fu, Z., Tang, M., Yang, Y., Fan, W., Zhou, S., Tsymbal, E.Y., Qiu, X.: Efficient perpendicular magnetization switching by a magnetic spin Hall effect in a noncollinear antiferromagnet. Nat. commun. **13**(1), 4447 (2022)
23. Kondou, K., Chen, H., Tomita, T., Ikhlas, M., Higo, T., MacDonald, A.H., Nakatsuji, S., Otani, Y.: Giant field-like torque by the out-of-plane magnetic spin Hall effect in a topological antiferromagnet. Nat. commun. **12**(1), 6491 (2021)
24. Qin, L., Xie, Y., Zhu, Z.Z., Tu, Y., Long, J., Gao, C., Zhang, Y., Cai, J.W., Liu, T., Li, E.: Measuring induced inverse spin Hall effect using an air-substrate micro-strip waveguide device. J. Magn. Magn. Mater. **560**, 169600 (2022)
25. Hazra, B.K., Pal, B., Jeon, J.C., Neumann, R.R., Göbel, B., Grover, B., Deniz, H., Styervoyedov, A., Meyerheim, H., Mertig, I., Yang, S.H., Parkin, S.S.: Generation of out-of-plane polarized spin current by spin swapping. Nat. Commun. **14**(1), 4549 (2023)
26. Deng, Y., Liu, X., Chen, Y., Du, Z., Jiang, N., Shen, C., Zhang, E., Zheng, H., Liu, H., Wang, K.: All-electrical switching of a topological non-collinear antiferromagnet at room temperature. Natl. Sci. Rev. **10** (2), nwac154 (2023)
27. Ikhlas, M., Tomita, T., Koretsune, T., Suzuki, M.T., Nishio-Hamane, D., Arita, R., Otani, Y., Nakatsuji, S.: Large anomalous Nernst effect at room temperature in a chiral antiferromagnet. Nat. Phys. **13**(11), 1085–1090 (2017)
28. Higo, T., Li, Y., Kondou, K., Qu, D., Ikhlas, M., Uesugi, R., Hanmane, D.N., Chien, C.L., Otani, Y., Nakatsuji, S.: Omnidirectional control of large electrical output in a topological antiferromagnet. Adv. Funct. Mater. **31**(15), 2008971 (2021)
29. Gao, D., Peng, Z., Zhang, N., Xie, Y., Yang, Y., Yang, W., Xia, S., Yan, W., Deng, L., Liu, T., Qin, J., Zhong, X., Bi, L.: Epitaxial growth of high quality Mn_3Sn thin films by pulsed laser deposition. Appl. Phys. Lett. **121** (24) (2022)
30. Chen, T., Tomita, T., Minami, S., Fu, M., Koretsune, T., Kitatani, M., Kitatani, M.K., Muhammad, I., Hanmane, D.N., Ishii, F., Arita, R., Nakatsuji, S.: Anomalous transport due to Weyl fermions in the chiral antiferromagnets Mn_3X, X= Sn. Ge. Nat. Commun. **12**(1), 572 (2021)
31. Bangar, H., Khan, K.I.A., Kumar, A., Chowdhury, N., Muduli, P.K.: Large spin hall conductivity in epitaxial thin films of kagome antiferromagnet Mn_3Sn at room temperature. Adv. Quantum Technol. **6**(1), 2200115 (2023)
32. Yu, T., Wu, H., He, H., Guo, C., Fang, C., Zhang, P., Wong, K. L., Xu, S., Han, X., Wang, K. L.: Large spin to charge conversion in antiferromagnetic Weyl semimetal Mn_3Sn. APL Mater. **9** (4) (2021)
33. Mosendz, O., Pearson, J.E., Fradin, F.Y., Bauer, G.E.W., Bader, S.D., Hoffmann, A.: Quantifying spin Hall angles from spin pumping: experiments and theory. Phys. Rev. Lett. **104**(4), 046601 (2010)
34. Deorani, P., Son, J., Banerjee, K., Koirala, N., Brahlek, M., Oh, S., Yang, H.: Observation of inverse spin Hall effect in bismuth selenide. Phys. Rev. B **90**, 094403 (2014)
35. Ruiz-Calaforra, A., Brächer, T., Lauer, V., Pirro, P., Heinz, B., Geilen, M., Chumak, A. V., Conca, A., Leven, B., Hillebrands, B.: The role of the non-magnetic material in spin pumping and magnetization dynamics in NiFe and CoFeB multilayer systems. J. Appl. Phys. **117** (16) (2015)
36. Kittel, C.: On the theory of ferromagnetic resonance absorption. Phys. Rev. Lett. **73**(2), 155 (1948)
37. Bansal, R., Muduli, P.K.: Investigation of magnetization dynamic damping in NiFe/Pd bilayer at room temperature. Mater. Today **28**, 308–310 (2020)